processes

MDPI

Article

Water Cleaning by a Continuous Fixed-Bed Column for Cr(VI) Eco-Adsorption with Green Adsorbent-Based Biomass: An Experimental Modeling Study

Mohammed Kebir [1,2], Hichem Tahraoui [3], Malika Chabani [2], Mohamed Trari [4], Nasrallah Noureddine [2], Aymen Amin Assadi [5], Abdeltif Amrane [5,*], Naoufel Ben Hamadi [6] and Lotfi Khezami [6]

1 Research Unit on Analysis and Technological Development in Environment (UR-ADTE/CRAPC), BP 384 Bou-Ismail, Tipaza 42000, Algeria
2 Laboratory of Reaction Engineering, Faculty of Mechanical Engineering and Process Engineering (USTHB), BP 32, Algiers 16111, Algeria
3 Laboratoire de Biomatériaux et Phénomènes de Transports (LBMPT), Université Yahia Fares de Médéa Pôle Urbain, Médéa 26000, Algeria
4 Laboratory of Storage and Valorization of Renewable Energies, Faculty of Chemistry (USTHB), BP 32, Algiers 16111, Algeria
5 Ecole Nationale Supérieure de Chimie de Rennes, CNRS, ISCR (Institut des Sciences Chimiques de Rennes)–UMR 6226, Univ Rennes, F-35000 Rennes, France
6 Department of Chemistry, Imam Mohammad Ibn Saud Islamic University (IMISIU), P.O. Box 5701, Riyadh 11432, Saudi Arabia
* Correspondence: abdeltif.amrane@univ-rennes1.fr; Tel.: +33-02-2323-4004

Abstract: In this study, chromate adsorption onto red peanut skin (RPS) was investigated in a fixed-bed column; FTIR, PZC, SEM, DLS, and BET were used to evaluate its adsorption properties. The experiments were conducted to determine the effect of physical parameters, including the inlet initial Cr(VI) concentration (100–500 mg L^{-1}), bed height (10–20 cm), and feed flow rate (13.59–23.45 mL min^{-1}). They were carried out to predict breakthrough curves. The adsorption capacity coefficients were determined using the most widely used Bohart–Adams model. It was tested to fit experimental data, for a better understand the dynamic behavior, and for further optimize column performance. It was found that the Cr(VI) uptake decreases when increasing the flow rate and that high chromate concentration and bed height consequently increase the column's life span. A high column adsorption capacity can be achieved with a higher Cr(VI) concentration due to the higher driving force. The results indicated that the Bohart–Adams model provides a good description ($R^2 > 0.98$) of the experimental data of the Cr(VI)'s removal from the aqueous solution on the RPS suggesting that the surface diffusion is the rate-limiting step in the continues adsorption process.. Breakthrough adsorption capacity is crucial for comparing RPS with other similar materials. Indeed, possible mechanisms have been suggested for illustrating adsorption onto RPS. The obtained results showed significant potential of 26.23 mg g^{-1} of RPS on Cr(VI) elimination at a natural pH of 5.35. Furthermore, this global investigation allowed for the design of a promising low-cost material for the future scale-up of cleaning wastewater polluted by metal and determine the properly conditions for operating column adsorption. This material provides an economical, efficient means of eliminating pollutants, thus meeting the main aims of the UN Sustainable Development Goals (UN SDGs).

Keywords: process modeling; chromate; eco-adsorption; red peanut skin; fixed bed; wastewater

Citation: Kebir, M.; Tahraoui, H.; Chabani, M.; Trari, M.; Noureddine, N.; Assadi, A.A.; Amrane, A.; Ben Hamadi, N.; Khezami, L. Water Cleaning by a Continuous Fixed-Bed Column for Cr(VI) Eco-Adsorption with Green Adsorbent-Based Biomass: An Experimental Modeling Study. *Processes* **2023**, *11*, 363. https://doi.org/10.3390/pr11020363

Academic Editor: Monika Wawrzkiewicz

Received: 3 November 2022
Revised: 11 January 2023
Accepted: 20 January 2023
Published: 24 January 2023

1. Introduction

The growth in urban populations has led to overall lifestyle changes and a significant development of activities, resulting in the over-exploitation of groundwater. Consequently, their risks impacted public health and led to a parallel increase in the regeneration of

harmful contamination-loaded substances released into the natural environment, such as those from mining, agricultural, and domestic activities [1].

The presence of hexavalent chromium in the aquatic environment has received considerable attention from scientists and engineers because of its widespread use in metallurgy and high toxicity [2], inevitably leading to the progressive degradation of the quality of clean water sources, which are lacking worldwide. Moreover, Cr(VI), either in the form of CrO_4^{2-} or $Cr_2O_7^{2-}$, accumulates in living organisms, causing severe damage to aquatic plants and animals and presenting a serious threat to the ecosystem. Cr(VI) is not biodegradable and must be removed from the source before its discharge into an aquatic medium, but conventional treatment technologies can generate a large quantity of toxic sludge and are not economical.

Pollution primarily arises from industrial activities such as leather tanning, cement making, pigmenting, and electroplating [3]. Conventional methods for chromium removal, including chemical precipitation, reverse osmosis, ion exchange, and biological and electroreduction, are expensive, especially when applied to high-flow effluents [4]. However, they are inefficient at low concentrations, and they often do not meet the standards for drinking water established by the World Health Organization, which restricts the maximum level to 0.3 mg L^{-1} [5].

Compared to other water cleaning processes, adsorption is considered the safest, simplest, most affordable, and most versatile technique for retaining these pollutants [6]. Nevertheless, a practical, effective metal removal method remains a significant environmental protection challenge [7]. Over the last few years, there has been much interest in environmentally friendly technologies for water purification [8]. Therefore, using natural biomasses as adsorbents for chromate removal is attractive. These biomasses include coconut coir pith [9], jute fiber (PANI-Jute) [10], acid-modified waste-activated carbons [11], cetyl tri methyl ammonium bromide [12], olive oil industry waste [13], chitosan Fe° nanoparticles [14], synthesized chitosan resin [15], chitosan-bond FeC nanoparticles [16], and xanthated chitosan [17].

Red peanut skin (RPS) is an attractive lignocellulosic adsorbent biomass with a rich surface grouping structure, allowing for interesting shape selectivity and an appreciable specific surface [18]. The proposed approach can be used effectively to keep the effluent concentration well below the permissible limit and to ensure the minimum solid waste management of toxic metal-loaded adsorbents. Although it usually has an appreciable uptake capacity, its availability and low cost are advantageous. It is also locally available and does not require pretreatment.

In this study, the dynamic adsorption process was applied for Cr(VI) removal using an RPS biomass in a fixed-bed column. The main objective of the present study was to evaluate the effect of various operating variables, such as the adsorbate concentration inlet rate, the initial Cr(VI) concentration, and the bed height, on the dynamic performance study. Next, the mathematical modeling using the empirical model of Bohart–Adams is applied to analyze the obtained data and predict the dynamic adsorption of the column and the breakthrough curve. To our knowledge, removing Cr(VI) by RPS biomass in a fixed-bed column has never been performed. The contribution of the main possible mechanism of Cr(VI) adsorption will be discussed.

2. Materials and Methods

2.1. Chemicals

All the chemicals and reagents used in the study were supplied from standard sources and were purely analytical. Potassium dichromate ($K_2Cr_2O_7$, Merck, 98%), sulfuric acid (H_2SO_4, Merck Millipore, 95–97%), hydrochloric acid (HCl, Biochem, 37%), sodium hydroxide (NaOH, Sigma Aldrich, 98%), and nitric acid (HNO_3; 70%) were acquired from Merck. Freshly used deionized water was used to prepare the experiments.

2.2. Preparation of Adsorbent Material

The biomass RPS used as an adsorbent was acquired from a south Algerian farm. It was thoroughly rinsed with double distilled water to remove dust impurities and dried at 40 °C overnight until a constant weight was reached. The sample was then ground in a mechanical grinder, and the powder was kept in glass bottles for further use.

2.3. Characterization of the Biomass Adsorbent

The biomass adsorbent RPS was characterized using various techniques. As previously noted, these techniques were its zero-point charge [19]. Next, a chemical elemental composition analysis was performed using X-ray fluorescence spectrometry (XRF), Rijuka Zsxpriness II, and Fourier Transform Infrared Spectroscopy (ATR–FTIR) with a range of 4000–400 cm^{-1} using a Bruker Alpha 1 spectrometer.

The pore size distribution of raw RPS powder was determined by dynamic light scattering DLS or quasi-elastic light scattering technique in the size range of 0.3 nm to 8 µm, the mean diameter was measured using Horiba Scientific SZ-100 Nanopartica series instruments in the suspension of water medium and based on the Brownian motion of particles. The raw RPS-specific surface area measurements were determined by N_2 adsorption–desorption at 77 K using a surface area analyzer (ASAP 2020 Micromeritics apparatus). Before gas adsorption analysis, the sample was outgassed at 393 K for 12 h [19].

The surface morphology and textural properties of the RPS samples before and after the Cr(VI) adsorption experiment were obtained using a scanning electron microscope (SEM) (FEI Quanta 200, SEM), the analysis was performed for the dried adsorbent powder before and after Cr(VI) adsorption in an air oven (Memmert, B200), thereafter it was positioned to stubs with double adhesive carbon discs, The SEM is operated with Normal secondary electron mode (SE) in low vacuum was used. A large field detector (LFD) at 10 kV acceleration voltage with a working distance of 10 mm, a spot size of 3.5 nm, a magnification of 6000 times and the analysis is portrayed in the photographs.

2.4. Continuous Flow Column Studies of Adsorption Experiments

The adsorption tests were conducted at room temperature in triplicate, and the mean values were considered for calculation. The continuous adsorption process was undertaken in a glass column with an internal diameter of 2 cm and a length of 50 cm. The adsorbent was backed in the column between two cotton plugs preventing the loss of particles. A glass ball prevented the washout of RPS, thus ensuring the homogeneous diffusion of the liquid.

The operating parameters that influence the Cr(VI) adsorption process of the column experiments are chosen based on our previous batch Cr(VI) adsorption part such as the bed height (Kebir et al., 2011). The solution of Cr(VI) initial concentration (100–500 mg L^{-1}) was continuously pumped using a peristaltic pump (Figure 1) at a fixed flow rate ranging from (13.59–23.45 mL min^{-1}) and the bed height (10–20 cm) where the height of 10 cm^{-1} correspond to 5 mg L^{-1} of RPS optimized dose in our previous study (Kebir et al., 2011). Throughout the process, the free pH (5.35) of the solution was kept constant for all the continuous study to become closer to the municipal wastewater. Aliquots were periodically withdrawn for analysis at different intervals of time until the saturation of the bed. The adsorption was followed by measuring the absorbance with a double beam spectrophotometer UV-Visible (Shimadzu 1800) using a 1 cm path-length quartz cell. Cr(VI) was then complexed with 1.5-diphenylcarbazide, and the value was taken at 540 nm, because high sensitivity of the photometric method, as we are working with high concentrations, the samples need to be diluted with distilled water and Cr(VI) concentration was determined from a calibration curve prepared with Cr(VI) standard solutions [20].

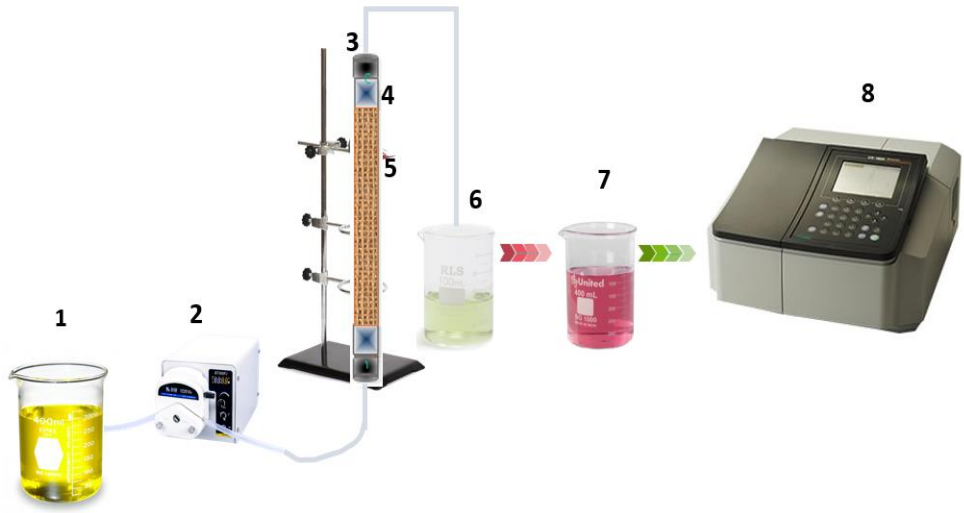

Figure 1. Schema of the experimental setup for the Cr(VI) fixed-bed adsorption. 1—Cr(VI) solution reservoir, 2—Peristaltic pump, 3—Cotton plugs, 4—Glass ball, 5—RPS fixed bed, 6—taken sample of Cr(VI), 7—Ready sample for analysis, 8—Spectrophotometer UV-Visible.

2.5. Fixed-Bed Column Kinetic and Mathematical Modeling

Adsorption operation is a complex process, and many variables govern its performance. A successful design of column adsorption requires the prediction of breakthrough curves for water treatment. Thus, the Bohart–Adams model was employed to fit the adsorption into fixed-bed configurations.

The Bohart-Adams Model

Due to its mathematical simplicity, the Bohart-Adams model has been used in many adsorption process-modeling studies. The Bohart-Adams model used for the description of the initial part of the breakthrough curve was based on surface reaction theory and mass transfer, assuming that the adsorption rate was proportional to both the adsorbent's residual capacity and the adsorbate's concentration [21–23]:

$$Ln(C/Co) = C_o t - K_{AB} N_o \left(\frac{Z}{U}\right) \quad (1)$$

where *Co* and *Ct* are the inlet and outlet adsorbate concentrations, respectively. Z (cm) is the bed height, U (cm min^{-1}) is the superficial velocity, N_o (mg L^{-1}) is the saturation concentration, and K_{AB} (L mg^{-1} min^{-1}) is the mass transfer coefficient. This model's advantage is its simplicity, and the characteristic parameters of the column were determined from the plot of *Ln(C/Co)* versus the reaction time (t).

3. Results

3.1. Adsorbent Characterization

3.1.1. Point of Zero Charge (PZC)

One of the essential characteristics of the adsorbent/liquid interface is the potential of zero either charge (PZC) to determine what pH range would be ideal for the adsorption of metals or organic compounds and whether deviation from the PZC would lead to the attraction of counterions to the surface. In this study, the biomass adsorbent RPS was evaluated, and its zero-point charge, as previously noted, was PZC = 6.15 [19].

In solutions containing metal and adsorbent, when the pH is greater than the PZC, the adsorbent surface is charged negatively, making it conducive to positive interaction with metallic species. However, when the pH of the medium solutions is lower than that of the PZC, the biomass surface is positively charged and can interact with negative species [3].

3.1.2. Chemical Composition

Fluorescence spectroscopy (XRF) was used to analyze the elemental composition of RPS before and after Cr(VI) adsorption. Each raw and adsorbed RPS sample was mixed with H_3BO_3 and subjected to XRF studies using a micro X-ray fluorescence (XRF) HORIBA brand-XGT model 5000 instrument. The composition, established by X-ray fluorescence, is shown in Table 1.

Table 1. Chemical composition of RPS biomass before and after Cr(VI) adsorption.

Element	Raw RPS (% Mass)	Adsorbed Cr(VI) (% Mass)
C	98.10	90.51
Na	0.04	0.04
Mg	0.35	0.28
Al	0.04	0.04
Si	0.06	0.06
P	0.13	0.12
S	0.17	0.16
Cl	0.04	0.05
K	0.60	3.59
Ca	0.35	0.34
Mn	0.01	0
Fe	0.02	0.02
Ni	0.0	0.01
Cu	0.01	0.01
Zn	0.06	0.05
Rb	0.01	0.01
Sr	0.01	0.01
Pb	0	0.06
Cr	0	4.66

Comparing the samples of raw RPS and Cr(VI) RPS after adsorption (Table 1), the concentration of K in the raw RPS was significantly lower than in the sample after Cr(VI) adsorption. This high concentration could have been due to using $K_2Cr_2O_7$ as a Cr(VI) source. The most abundant element in both RPS samples was C. Otherwise, the different behaviors of the elements were indicated. Some elements, such as Na, Mg, Zn and S, decreased slightly in the Cr(VI)-adsorbed RPS, while others, including Si, Al, Ca, Fe, Ni, Cu, Mn, Sr, Rb and Fe, remained nearly constant in all samples. Finally, Cr(VI) and K appeared significantly in the adsorbed RPS.

3.1.3. FTIR Analysis

The FTIR displayed several fundamental absorption bands (Figure 2a,b).

The broad, intense peak at 3292 and 3227 cm^{-1} corresponded to the O–H stretching vibrations of water, alcohol and carboxylic acids [24,25]. The peaks at 2921 and 2321 cm^{-1} were attributed to C–H stretching in the aliphatic group. The band at 2852 cm^{-1} was due to C–H's symmetrical and asymmetrical stretching vibration in the CH_2 groups [25], but the peak intensity at 1744 cm^{-1} was assigned to the stretching vibration of the C=O bond of the carboxylic groups. The peak at 1258 cm^{-1} was due to the ester group's C–O stretching vibration peak, and the peak at 1014 –1015 cm^{-1} was due to the vibration band of the C-Metal [26]. The bands at 808 cm^{-1} were the signature of Cr-linked with RPS groups [27]. The peaks at 533 and 512 cm^{-1} were attributed to the C–C and C–N ring deformation

out-of-plane bending vibrations [28]. This phenomenon was due to the bonds formed between Cr(VI) ions and the active sites of the RPS adsorbent [1].

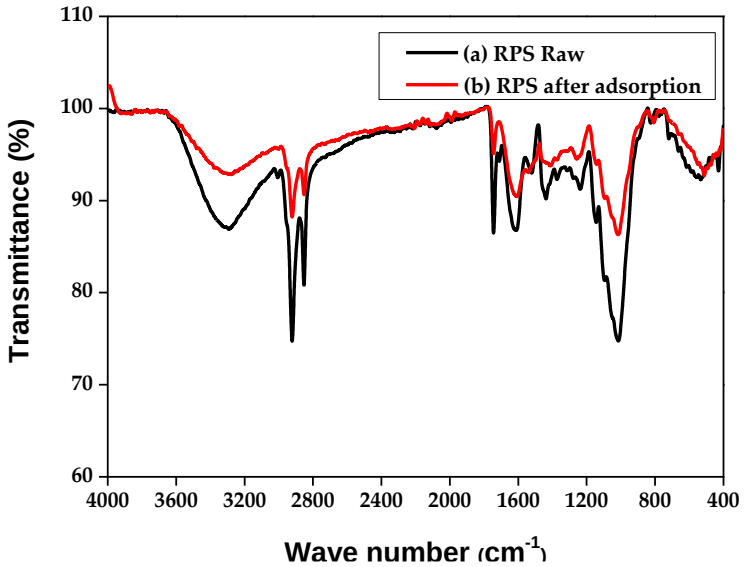

Figure 2. ATR-FTIR analysis of RPS before (**a**) and after adsorption (**b**).

The ATR-FTIR spectrum after Cr(VI) adsorption (Figure 2b) clearly showed a decrease in the intensity of the peaks compared to the peaks recorded before adsorption (Figure 2b), namely the following:

(1) The stretching vibration of O–H of the functional group of alcohols and carboxylic acids (3408.8 cm^{-1}).
(2) The C–H bending vibration of the stretching vibration CH_3 groups (2918.7, 1440.5, and 1373.42 cm^{-1}).
(3) The band at 1739.8 and 1630.9 cm^{-1} is relative to the C=O stretching of the carboxylic acid with an intermolecular hydrogen bond.

This result indicated that Cr(VI) could also be eliminated by RPS material and the shifts in peaks could be due to the involvement of hydroxyl, carbonyl and carboxylic groups in the adsorption process.

3.1.4. Surface Area and Pore Characteristics

The particle size distribution of raw RPS powder was determined by a dynamic light scattering technique at 25 °C (Figure 3). The obtained data were found to be almost equal to the mean particle size of 534 nm. In addition, this result clearly indicates that the particles are in monodispersed phase with very low chances of aggregation. The raw RPS-specific surface area measurements of the porosity and the pore volume were obtained from adsorption–desorption isotherms at 77 K, which indicated a Langmuir area of 2.52 $m^2\ g^{-1}$, a pore volume of 0.003 $cm^3\ g^{-1}$, an external surface area of 4.0158 $m^2\ g^{-1}$, and an average pore width of 40.2498 Å.

3.1.5. SEM Analysis

The morphology of the RPS before and after Cr(VI) adsorption was noted by SEM images and is illustrated in Figure 4a,b. Figure 4a,b shows that raw RPS presents on irregular, fibrous, and porous surfaces with different sizes typical of lignocellulosic materials, allowing for better heterogeneous Cr(VI) biosorption due to the extensive reach functional interface. Figure 3b depicts the SEM micrographs for RPS after the Cr(VI) adsorption experiments caused changes to the biomaterial morphology as mentioned by red circles. This change may imply that Cr(VI) ions were bound to the surface of RPS by an electrostatic attraction mechanism due to the chemical composition of RPS, as confirmed by XRF and

ATR analysis. This eventually became more compact. However, on the surface of the RPS (Figure 3b), agglomerations of Cr(VI) ions were observed, which may be attributed to the formation of micro-precipitated complexes or chelates on the RPS adsorbent's surface [29].

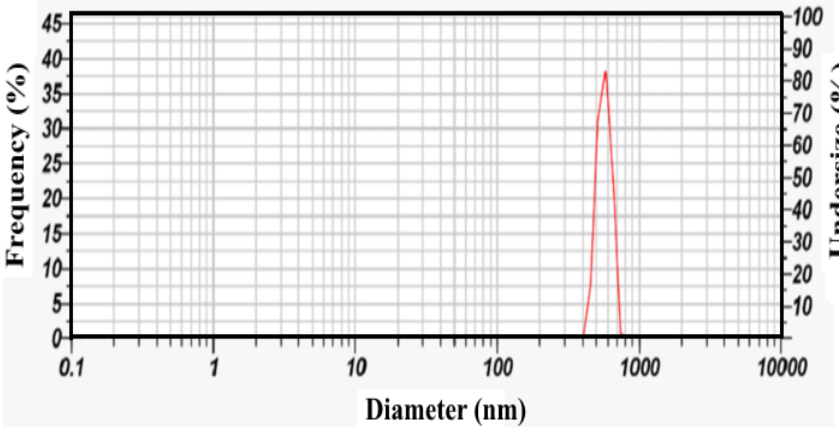

Figure 3. Particle size distribution of RPS by dynamic light scattering.

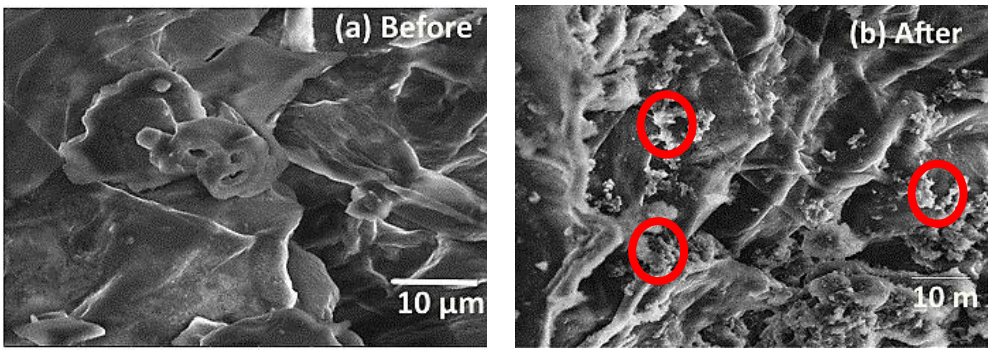

Figure 4. Micrographs from a scanning electron microscope of RPS before the adsorption process (**a**) and after Cr(VI) adsorption (**b**).

3.2. Governing Parameters

3.2.1. Effects of Cr(VI) Concentration

The breakthrough curve was obtained by changing the inlet Cr(VI) ions' concentration. The breakthrough curve point appeared more slowly, increasing the initial Cr(VI) concentration and decreasing the bed height.

The fixed-bed column experiments were conducted by varying Co in the range of 100–500 mg L^{-1} to determine its effect on the uptake performance of the breakthrough curve. The flow rate was fixed at 13.59 mL min^{-1}, feeding the column continually with a bed height of 10 cm. The corresponding breakthrough curves are shown in Figure 5. High feed concentration saturates RPS rapidly, thereby decreasing both the breakthrough (t_b) and the saturation point time (t_s), as previously observed by others [13]. The breakthrough and exhaustion times for a concentration of 100 mg L^{-1} were 27 and 120.5 min, respectively, and decreased to 25 and 104.73 min for 200 mg L^{-1}. The adsorption capacities obtained by integrating the area above the breakthrough curve were 4.597 and 4.603 mg g^{-1}. The decrease in the breakthrough and the exhaustion times at high concentrations of Co were due to the rapid exhaustion of the adsorption sites. The high concentration also provided the driving force for the transfer process, which overcame the mass transfer resistance between the adsorbent and the solution, resulting in better column performance. However, the breakthrough curve was dispersed and slowed down at low concentrations of Co. In contrast, the bed saturation was faster at high concentrations, resulting in the rapid exhaustion of sorption sites and making the Cr(VI) uptake less efficient.

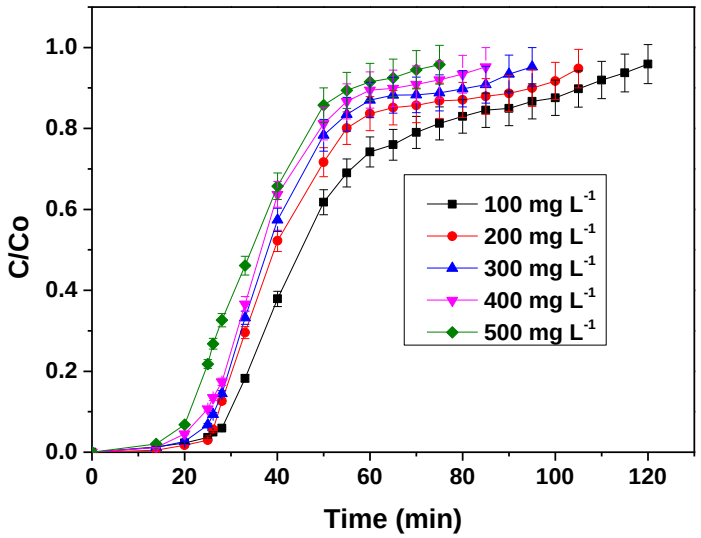

Figure 5. Effect of initial concentration on breakthrough curves.

The breakthrough was flat for low inlet concentrations, indicating a relatively wide mass transfer zone and film-controlled process. Conversely, the breakthrough curves were sharp at high Cr(VI) concentrations, implying a smaller mass transfer zone and intra-particle diffusion control. Many authors have reported similar observations [23,30].

3.2.2. Effects of Bed Height

To investigate the effect of bed height on the breakthrough curves for Cr(VI) adsorption onto RPS, three masses of adsorbent were used (5, 7.5, and 10 g), producing heights of 10, 15, and 20 cm, respectively, under the following operating conditions: 13.25 mL min^{-1}; Co = 300 mg L^{-1}, pH 5.35, and 25 °C. The typical curves are shown in Figure 6. It was noted that the Cr(VI) uptake increased when the height was raised from 10 to 20 cm, but both the breakthrough and the exhaustion point time increased since more binding sites were available for Cr(VI) adsorption. Consequently, more liquid could be treated, and higher contact times would result in a broadened mass transfer zone. As the bed height increased, a steeper breakthrough curve was observed.

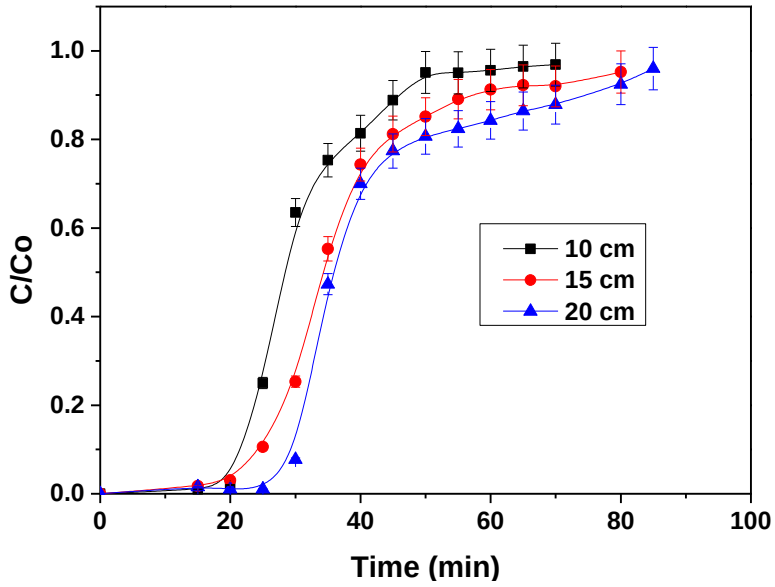

Figure 6. Effect of bed height on breakthrough curves.

The increase in the breakthrough and exhaustion times in adsorption by increasing the bed depth was due to the increased amount of RPS, which provided more functional sites for the Cr(VI) ions [31].

The amount of RPS packed in the column varied with bed height. It was also found that the metal uptake decreased slightly when the bed height decreased. This finding may have been due to the effect of liquid maldistribution and channeling in the tall beds.

3.2.3. Effect of the Flow Rate

The flow-rate effect on Cr(VI) adsorption was investigated at 13.25, 18.53 and 23.45 mL min^{-1} for a height of 10 cm and a pH of 5.35. The breakthrough curves are illustrated in Figure 7. The adsorption efficiency was higher at low flow rates, and a breakthrough point was rapidly attained. Such behavior was due to insufficient residence time, resulting in fewer Cr(VI) ions on the bed column and, thus, due to the diffusion limitation of the solute in the adsorbent pores [32]. Even though a shortened mass transfer zone was observed for the highest flow rate, the Cr(VI) removal percentage and the Cr(VI) uptake were highest at a low flow rate (13.25 mL min^{-1}).

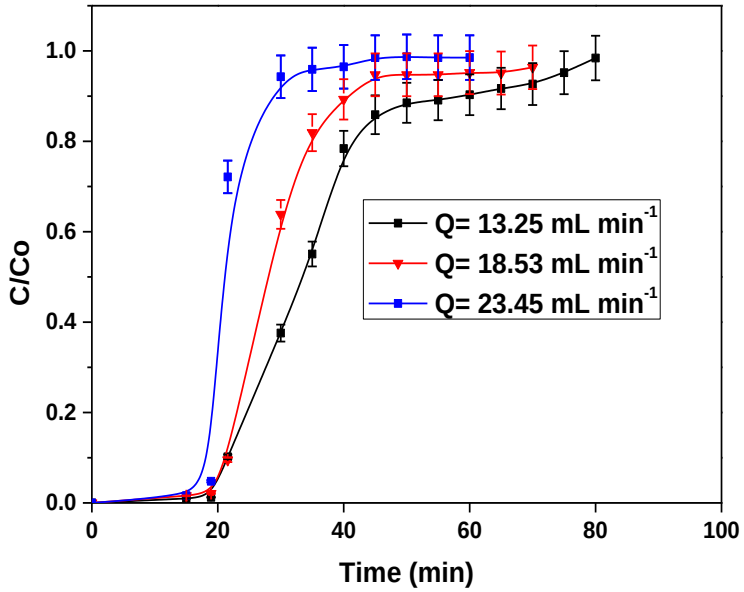

Figure 7. Effect of the flow rate on breakthrough curves.

The equilibrium column capacity of RPS quickly reached its maximum value at a higher flow rate because more Cr(VI) ions exchanged with functional group sites in a shorter time.

3.3. The Bohart-Adams Model

The Bohart-Adams model was applied to describe the initial part of the breakthrough curve. It focused on characteristic parameters, such as the maximum adsorption capacity No and the mass transfer coefficient K_{AB}. The curves ln(Ct/Co) were plotted against the time (t) at various flow rates, Co and h. The comparison of the experimental data with the predicted breakthrough curves is illustrated in Figure 8a–c, and the calculated values are provided in Table 2.

Table 2 indicates that the values of N_o increased with the inlet concentration from 2163.98 to 4932.23 m L^{-1}, and the volumetric flow rate increased from 4693.46 to 5416.24 m L^{-1}, as it decreased from 2610.58 to 2514.30 for the increased the bed height.

This could be explain that, the increase in No with increasing initial Cr(VI) concentration and the feed flow rate results in a higher effluent concentration; this is because a large number of molecules leave the column without treatment, in addition to the higher saturation of RPS adsorbent sites. This adsorption was directed to earlier bed saturation,

thus reducing N_o [33]. Furthermore, an increase in the constant K_{AB} by increasing the flow rate and a decrease with the rise of the initial Cr(VI) concentration and flow rate indicated that the external mass transfer dominated the overall kinetic system.

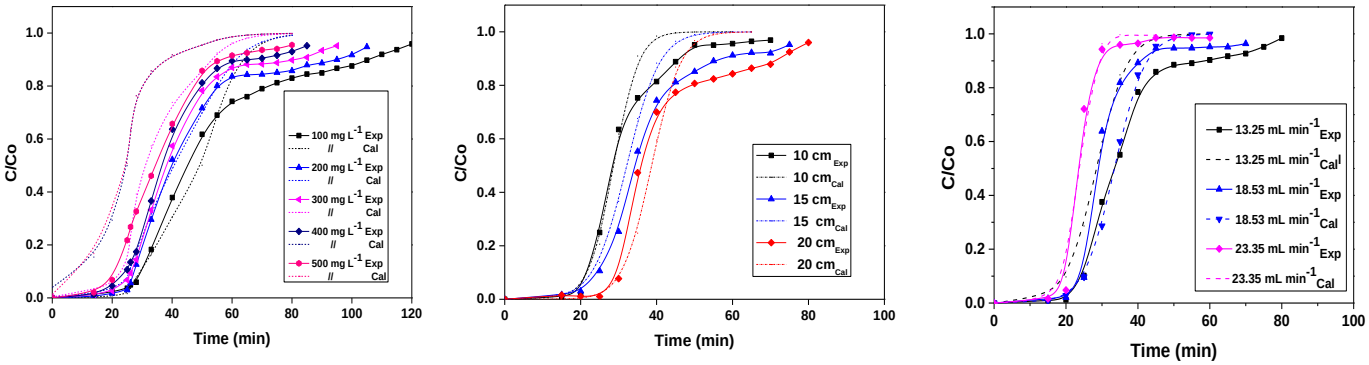

Figure 8. A comparison of the experimental and predicted breakthrough curves obtained at different initial Cr(VI) concentrations (**a**), different bed heights (**b**) and different flow rates (**c**), according to the Bohart-Adams model.

Table 2. The parameters of the Bohart–Adams model for different initial concentrations, flow rates and bed heights.

Operating Conditions		Bohart-Adams Model Parameters		
		N_o (m L^{-1})	K_{AB} (L $mg^{-1}min^{-1}$)	R^2
Concentration (mg L^{-1})	100	2163.98	0.0016	0.785
	200	3865.08	0.0006	0.983
	300	4932.2 3	0.0004	0.988
	400	4432.11	0.0003	0.905
Flow rate (mL min^{-1})	13.25	4693.46	0.0006	0.970
	18.53	5416.24	0.0008	0.952
	23.35	5353.35	0.0028	0.956
Bed height (cm)	10	2610.58	0.0017	0.957
	15	1940.37	0.0012	0.946
	20	2514.30	0.0010	0.911

3.4. Comparison of Adsorption Capacity with That of Other Absorbents in the Literature

To evaluate the effect of RPS capacity on Cr adsorption, the results obtained in this study were compared with other adsorbents in the literature. A comparison of adsorption capacity at the defined pH is shown in Table 3.

From Table 3, researchers [13–16] used different forms of chitosan, such as xanthated chitosan, chitosan-bond FeC nanoparticles, synthesized chitosan resin, and chitosan Fe° nanoparticles, for Cr removal. The adsorption capacity results were very high for the adsorbents xanthated chitosan (202.25 mg g^{-1} with a pH adjustment of 3) and synthesized chitosan resin (100.9 mg g^{-1} with a pH adjustment of 3.5). In contrast, the adsorption capacity of chitosan-bonded FeC nanoparticles and chitosan Fe° nanoparticles was 10.5 mg g^{-1} at pH 7.5 and 32 mg g^{-1} at pH 6.

In a previous study [10], acid-modified waste-activated carbons used as adsorbents obtained a very high adsorption capacity, with a value of 288.19 mg g^{-1} at pH 3.

Conversely, the use of adsorbent materials, such as jute fiber (PANI-Jute), cetyl tri methyl ammonium bromide, and olive oil industry waste (Table 3), gave a very low Cr(VI) adsorption capacity that did not exceed 4.66 mg g^{-1} in an acid range of pH 1–3.

Table 3. Comparison of the Cr(VI) adsorption capacity of different adsorbents.

Materials	Adsorption Capacity (mg g^{-1})	pH	References
Jute fiber (PANI-Jute)	4.66	3	[9]
Acid modified waste activated carbons	288.19	3	[10]
Cetyl tri methyl ammonium bromide	0.366	1.15–1.39	[12]
Olive oil industry waste	3.33	1–2	[13]
Chitosan Fe° Nanoparticles	32	6	[14]
Synthesized chitosan Resin	100.9	3.5	[15]
Chitosan-bond FeC nanoparticules	10.5	7.5	[16]
Xanthated chitosan	202.25	3	[17]
RPS	26.21	5.35	This work

Comparing these results with the RPS capacity used in this work, which gave 26.21 mg g^{-1} at a natural pH of 5.35, represents an advantage because the effluent does not require neutralization treatment. This capacity could provide a solution for small- and medium-sized businesses to clean their effluents before discharging them into the environment. Using chitosan in different forms or activated carbon also provides interesting results compared to RPS [31]. However, we found that if it is necessary to consume chemicals, thermal energy, and thereby contaminated water while reducing operating costs, using RPS was the best solution because chitosan requires extraction by shrimp shell waste [34] and *Goliathus orientalis* [35].

These data show the benefits of using RPS for eco-adsorption with green adsorbents. Ultimately, the study showed the advantages of using RPS as a potential green, eco-friendly adsorbent for cleaning wastewater contaminated with Cr(VI) metal in a column mode while offering opportunities for future industrial use.

3.5. Cr(VI) Adsorption on RPS Mechanisms

As previous studies have indicated, the adsorption of Cr(VI) containing aqueous solutions onto natural material is a complex process involving the binding of metal ions by a variety of physical and chemical interactions, including precipitation, complexation precipitation, electrostatic attractiveness, ion exchange, reduction, chemisorption, and adsorption on the pores and surface [34,36]. Figure 9 shows the different mechanisms involved in Cr(VI) adsorption onto RPS. Due to natural biomass adsorbents' complex elementary composition, they contain several compounds, such as cellulose, hemicellulose, lignin, simple sugar, starches, proteins and hydrocarbons; several functional groups, including alcohols, carbonyls, sulfonates, carbonyls, amides and carboxylic acids; and esters that can attract metal ions, which is the bath way that governs this adsorption process [37–43].

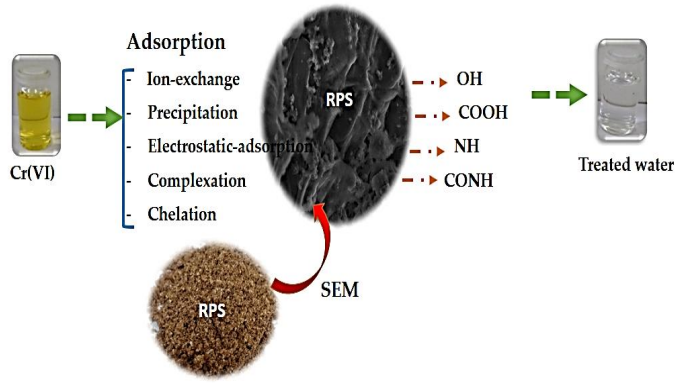

Figure 9. A schematic diagram of the mechanism of the RPS adsorbent for removing Cr(VI).

4. Conclusions

The present work reveals the efficiency of dynamic adsorption of the red peanut skin aa a green and inexpensive process in eliminating Cr(VI) ions in the aqueous medium. Results showed that the Cr(VI) ions adsorption is dependent on the flow rate, inlet Cr(VI) concentration and bed height.

The study also evaluated the breakthrough curve, which is significantly affected by the Cr(VI) initial concentration, the flow rates and the bed height. Additionally, Cr(VI) ions adsorption on RPS in a fixed bed column is a low-cost technique. Such configuration operates better at weak Cr(VI) concentrations, and low flow rates. The Bohart-Adams model provides simple and comprehensive approaches for evaluating the sorption column tests. However, their validity remains limited to the operating conditions such as inlet concentrations, low feed flow rate and bed height.

- The modeling of the whole breakthrough curves is applied with successful with the Bohart–Adams model, indicating that the surface diffusion is the rate-limiting step in the continues adsorption process, and the latter can be used with confidence of the purpose of design; also, it is the most suitable to fit the experimental results.
- The comparison of the adsorption capacity of RPS adsorbent for Cr(VI) with the adsorbents attempted in fixed-bed columns. It may be concluded that the current green adsorbent has a highly comparable adsorption capacity.
- The Cr(VI) adsorption mechanism onto RPS is complex and takes place since it involves several steps, the electrostatic interaction between the adsorbent functional groups and the Cr(VI) ions make up the adsorption mechanism.
- The data in this investigation of red peanut skin for adsorbing Cr(VI) respond perfectly to the requirements of the global sustainable development policy. Namely, affordability and innovation to combat climate change, as stipulated in the Sustainable Development Goals 7 and 9, which target clean and affordable energy and industry, innovation and infrastructure.

Author Contributions: Conceptualization, M.K. and H.T.; methodology, M.K.; software, M.K.; validation, M.C., M.T. and M.K.; formal analysis, M.K. and H.T.; investigation, A.A.A.; resources, L.K.; data curation, M.K.; writing—original draft preparation, M.K.; writing—review and editing, A.A.A.; A.A. and N.B.H.; visualization, N.N.; supervision, N.N.; project administration, A.A.; funding acquisition, M.K. and N.B.H. All authors have read and agreed to the published version of the manuscript.

Funding: This research was funded by Imam Mohammad Ibn Saud Islamic University (IMSIU): Research Partnership Program no RP-21-09-66.

Data Availability Statement: Not applicable.

Acknowledgments: The authors extend their appreciation to the Deanship of Scientific Research at Imam Mohammad Ibn Saud Islamic University (IMSIU) for funding and supporting this work through Research Partnership Program no RP-21-09-66.

Conflicts of Interest: The authors declare no conflict of interest.

References

1. Zhuang, J.; Li, M.; Pu, Y.; Ragauskas, A.; Yoo, C. Observation of Potential Contaminants in Processed Biomass Using Fourier Transform Infrared Spectroscopy. *Appl. Sci.* **2020**, *10*, 4345. [CrossRef]
2. Yousef, R.; Qiblawey, H.; El-Naas, M.H. Adsorption as a Process for Produced Water Treatment: A Review. *Processes* **2020**, *8*, 1657. [CrossRef]
3. Younas, F.; Mustafa, A.; Farooqi, Z.U.R.; Wang, X.; Younas, S.; Mohy-Ud-Din, W.; Ashir Hameed, M.; Mohsin Abrar, M.; Maitlo, A.A.; Noreen, S.; et al. Current and Emerging Adsorbent Technologies for Wastewater Treatment: Trends, Limitations, and Environmental Implications. *Water* **2021**, *13*, 215. [CrossRef]
4. Yarwood, J.; Douthwaite, R.; Duckett, S. *Spectroscopic Properties of Inorganic and Organometallic Compounds: Techniques, Materials and Applications*; Royal Society of Chemistry: Cambridge, UK, 2010; Volume 41, ISBN 978-1-84755-047-7.
5. Yakout, S.M.; Hassan, M.R.; Omar, H.A. Fixed-Bed Column Study for the Removal of Hexavalent Chromium Ions from Aqueous Solutions via Pyrolysis of the Rice Husk. *DWT* **2019**, *170*, 128–137. [CrossRef]

6. Xu, L.; Cui, H.; Zheng, X.; Liang, J.; Xing, X.; Yao, L.; Chen, Z.; Zhou, J. Adsorption of Cu^{2+} to Biomass Ash and Its Modified Product. *Water Sci. Technol.* **2018**, *2017*, 115–125. [CrossRef]
7. Wu, Y.; Jiang, Y.; Han, D.; Wang, F.; Zhu, J. Speciation of Chromium in Water Using Crosslinked Chitosan-Bound FeC Nanoparticles as Solid-Phase Extractant, and Determination by Flame Atomic Absorption Spectrometry. *Microchim. Acta* **2007**, *159*, 333–339. [CrossRef]
8. Tielong, L.; Bing, G.; Na, Z.; Zhaohui, J.; Xinhua, Q. Hexavalent Chromium Removal from Water Using Chitosan-Fe^0 Nanoparticles. *J. Phys. Conf. Ser.* **2009**, *188*, 012057. [CrossRef]
9. Tejada-Tovar, C.; Gonzalez-Delgado, A.D.; Villabona-Ortiz, A. Characterization of Residual Biomasses and Its Application for the Removal of Lead Ions from Aqueous Solution. *Appl. Sci.* **2019**, *9*, 4486. [CrossRef]
10. Sulaymon, A.H.; Abid, B.A.; Al-Najar, J.A. Removal of Lead Copper Chromium and Cobalt Ions onto Granular Activated Carbon in Batch and Fixed-Bed Adsorbers. *Chem. Eng. J.* **2009**, *155*, 647–653. [CrossRef]
11. Suksabye, P.; Thiravetyan, P.; Nakbanpote, W. Column Study of Chromium(VI) Adsorption from Electroplating Industry by Coconut Coir Pith. *J. Hazard. Mater.* **2008**, *160*, 56–62. [CrossRef]
12. Rajesh, N.; Deepthi, B.; Subramaniam, A. Solid Phase Extraction of Chromium(VI) from Aqueous Solutions by Adsorption of Its Ion-Association Complex with Cetyltrimethylammoniumbromide on an Alumina Column. *J. Hazard. Mater.* **2007**, *144*, 464–469. [CrossRef] [PubMed]
13. Padmesh, T.V.N.; Vijayaraghavan, K.; Sekaran, G.; Velan, M. Batch and Column Studies on Biosorption of Acid Dyes on Fresh Water Macro Alga Azolla Filiculoides. *J. Hazard. Mater.* **2005**, *125*, 121–129. [CrossRef] [PubMed]
14. Nag, S.; Bar, N.; Das, S.K. Cr(VI) Removal from Aqueous Solution Using Green Adsorbents in Continuous Bed Column—Statistical and GA-ANN Hybrid Modelling. *Chem. Eng. Sci.* **2020**, *226*, 115904. [CrossRef]
15. Moreno-Benavides, J.A.; Peña-Salamanca, E.J.; Benítez-Campo, N. Reducing $Cr6^+$ in Electroplating Wastewater with Bacillus Cereus Strain BUniv. *Science* **2019**, *24*, 73–89. [CrossRef]
16. Mondal, N.K.; Samanta, A.; Chakraborty, S.; Shaikh, W.A. Enhanced Chromium(VI) Removal Using Banana Peel Dust: Isotherms, Kinetics and Thermodynamics Study. *Sustain. Water Resour. Manag.* **2018**, *4*, 489–497. [CrossRef]
17. Mignardi, S.; Archilletti, L.; Medeghini, L.; De Vito, C. Valorization of Eggshell Biowaste for Sustainable Environmental Remediation. *Sci. Rep.* **2020**, *10*, 2436. [CrossRef]
18. Martínez-Huitle, C.A. Environment-Friendly Electrochemical Processes. *Materials* **2021**, *14*, 1548. [CrossRef]
19. Malkoc, E.; Nuhoglu, Y.; Dundar, M. Adsorption of Chromium(VI) on Pomace—An Olive Oil Industry Waste: Batch and Column Studies. *J. Hazard. Mater.* **2006**, *138*, 142–151. [CrossRef]
20. Mahringer, D.; Polenz, C.; El-Athman, F. Stabilization of Chromium (VI) in the Presence of Iron (II): Method Development and Validation. *Water* **2020**, *12*, 924. [CrossRef]
21. Liu, L.; Cao, L.; Niu, H.; Wang, J. Zinc Metal–Organic Framework Growing on the Surface of Fruit Peels and Its Photocatalytic Activity. *ACS Omega* **2021**, *6*, 10187–10195. [CrossRef]
22. Levason, W.; Reid, G.; Zhang, W. Synthesis, Properties, and Structures of Chromium(VI) and Chromium(V) Complexes with Heterocyclic Nitrogen Ligands: Chromium(VI) and Chromium(V) Complexes with Heterocyclic Nitrogen Ligands. *Z. Anorg. Allg. Chem.* **2014**, *640*, 35–39. [CrossRef]
23. Kumar, P.A.; Chakraborty, S. Fixed-Bed Column Study for Hexavalent Chromium Removal and Recovery by Short-Chain Polyaniline Synthesized on Jute Fiber. *J. Hazard. Mater.* **2009**, *162*, 1086–1098. [CrossRef] [PubMed]
24. Kromah, V.; Zhang, G. Aqueous Adsorption of Heavy Metals on Metal Sulfide Nanomaterials: Synthesis and Application. *Water* **2021**, *13*, 1843. [CrossRef]
25. Korus, A.; Szlęk, A.; Samson, A. Physicochemical Properties of Biochars Prepared from Raw and Acetone-Extracted Pine Wood. *Fuel Process. Technol.* **2019**, *185*, 106–116. [CrossRef]
26. Ko, D.C.K.; Porter, J.F.; McKay, G. Optimised Correlations for the Fixed-Bed Adsorption of Metal Ions on Bone Char. *Chem. Eng. Sci.* **2000**, *55*, 5819–5829. [CrossRef]
27. Kebir, M.; Trari, M.; Maachi, R.; Nasrallah, N.; Bellal, B.; Amrane, A. Relevance of a Hybrid Process Coupling Adsorption and Visible Light Photocatalysis Involving a New Hetero-System $CuCo_2O_4/TiO_2$ for the Removal of Hexavalent Chromium. *J. Environ. Chem. Eng.* **2015**, *3*, 548–559. [CrossRef]
28. Kebir, M.; Chabani, M.; Nasrallah, N.; Bensmaili, A.; Trari, M. Coupling Adsorption with Photocatalysis Process for the Cr(VI) Removal. *Desalination* **2011**, *270*, 166–173. [CrossRef]
29. Hu, Q.; Pang, S.; Wang, D.; Yang, Y.; Liu, H. Deeper Insights into the Bohart–Adams Model in a Fixed-Bed Column. *J. Phys. Chem. B* **2021**, *125*, 8494–8501. [CrossRef]
30. Gizaw, A.; Zewge, F.; Chebude, Y.; Mekonnen, A.; Tesfaye, M. Simultaneous Nitrate and Phosphate Abatement Using Calcium Silicate Hydrate Adsorbent: Fixed Bed Column Adsorption Study. *Surf. Interfaces* **2022**, *30*, 101961. [CrossRef]
31. Ghosh, P.K. Hexavalent Chromium [Cr(VI)] Removal by Acid Modified Waste Activated Carbons. *J. Hazard. Mater.* **2009**, *171*, 116–122. [CrossRef]
32. Furusho, Y.; Sabarudin, A.; Hakim, L.; Oshita, K.; Oshima, M.; Motomizu, S. Automated Pretreatment System for the Speciation of Cr(III) and Cr(VI) Using Dual Mini-Columns Packed with Newly Synthesized Chitosan Resin and ME-03 Resin. *Anal. Sci.* **2009**, *25*, 51–56. [CrossRef] [PubMed]

33. Fournier, P.; Szczepanski, C.R.; Godeau, R.-P.; Godeau, G. Chitosan Extraction from Goliathus Orientalis Moser, 1909: Characterization and Comparison with Commercially Available Chitosan. *Biomimetics* **2020**, *5*, 15. [CrossRef] [PubMed]
34. Emami Moghaddam, S.A.; Harun, R.; Mokhtar, M.N.; Zakaria, R. Potential of Zeolite and Algae in Biomass Immobilization. *BioMed Res. Int.* **2018**, *15*, 6563196. [CrossRef]
35. da Costa, T.B.; da Silva, T.L.; Costa, C.S.D.; da Silva, M.G.C.; Vieira, M.G.A. Chromium Adsorption Using Sargassum Filipendula Algae Waste from Alginate Extraction: Batch and Fixed-Bed Column Studies. *Chem. Eng. J. Adv.* **2022**, *11*, 100341. [CrossRef]
36. Chu, K.H. Breakthrough Curve Analysis by Simplistic Models of Fixed Bed Adsorption: In Defense of the Century-Old Bohart-Adams Model. *Chem. Eng. J.* **2020**, *380*, 122513. [CrossRef]
37. Chauhan, D.; Sankararamakrishnan, N. Modeling and Evaluation on Removal of Hexavalent Chromium from Aqueous Systems Using Fixed Bed Column. *J. Hazard. Mater.* **2011**, *185*, 55–62. [CrossRef]
38. Charis, G.; Danha, G.; Muzenda, E. Characterizations of Biomasses for Subsequent Thermochemical Conversion: A Comparative Study of Pine Sawdust and Acacia Tortilis. *Processes* **2020**, *8*, 546. [CrossRef]
39. Abidi, M.; Hajjaji, A.; Bouzaza, A.; Trablesi, K.; Makhlouf, H.; Rtimi, S.; Assadi, A.A.; Bessais, B. Simultaneous removal of bacteria and volatile organic compounds on Cu2O-NPs dec-orated TiO_2 nanotubes: Competition effect and kinetic studies. *J. Photochem. Photobiol. A Chem.* **2020**, *400*, 112722. [CrossRef]
40. Baaloudj, O.; Nasrallah, N.; Kebir, M.; Khezami, L.; Amrane, A.; Assadi, A.A. A compara-tive study of ceramic nanoparticles synthesized for antibiotic removal: Catalysis charac-terization and photocatalytic performance modeling. *Environ. Sci. Pollut. Res.* **2021**, *28*, 13900–13912. [CrossRef]
41. Assadi, A.A.; Bouzaza, A.; Lemasle, M.; Wolbert, D. Removal of trimethylamine and iso-valeric acid from gas streams in a continuous flow surface discharge plasma reactor. *Chem. Eng. Res. Des.* **2015**, *93*, 640–651. [CrossRef]
42. Azzaz, A.A.; Jellali, S.; Akrout, H.; Assadi, A.A.; Bousselmi, L. Dynamic investigations on cationic dye desorption from chemically modified lignocellulosic material using a low-cost eluent: Dye recovery and anodic oxidation efficiencies of the desorbed solutions. *J. Clean. Prod.* **2018**, *201*, 28–38. [CrossRef]
43. Zeghioud, H.; Assadi, A.A.; Khellaf, N.; Djelal, H.; Amrane, A.; Rtimi, S. Reactive species monitoring and their contribution for removal of textile effluent with photocatalysis under UV and visible lights: Dynamics and mechanism. *J. Photochem. Photo-Biol. A Chem.* **2018**, *365*, 94–102. [CrossRef]